Electronic Supplementary Material (ESI) for RSC Advances.

Supplementary information:

The controllable fabrication of novel hierarchical nanosheet-assembled Bi_2MoO_6 hollow micronbox with ultra-high surface area for excellent solar to chemistry energy conversion

Chunjing Shi, Xiaoli Dong,*[a] Yuchen Hao, Xiuying Wang, Hongchao Ma and Xiufang Zhang

Experimental section:

All materials and chemicals were used as acquired without further purification. Firstly, 0.15g sodium oleate was dissolved in 20 ml hot ethylene glycol with strong stirring for 10 min. Then 210 mg bismuth nitrate and 50 mg sodium molybdate were quickly added into above solution, respectively. After stirring for about 35 min, 60 ml absolute ethyl alcohol was slowly injected into above mixed solution and still stirring for 40 min. Finally, the mixture was transferred into a 100 ml Teflon-lined autoclave, sealed and heated at 160 ^{o}C for 36 h. The product was allowed to cool down to room temperature naturally, and the resultant sample was obtained by centrifugally separated, washed with cyclohexane and absolute ethanol many times, and dried under vacuum condition. The production sample marked as B-Bi_2MoO_6. Moreover, the conventional large-sheet Bi_2MoO_6 was synthesized via a simple hydrothermal method. The solution solution A was first prepared by dissolving 1.0 mmol of $Bi(NO_3)_3{\cdot}5H_2O$ in 20 ml of EG with vigorous

stirring for 10 min. 0.5 mmol of $Na_2MoO_4 \cdot 2H_2O$ were dissolved in 20 ml of deionized H_2O and marked as solution B. When solution A and B became clear, the two solutions were mixed and stirred for 2 h until the resulting mixture became homogeneous. Then, the homogeneous suspension was sealed in a 50 mL Teflon-lined autoclave, sealed and heated at 180 °C for 4 h and then cooled to room temperature naturally. The precipitate was collected by centrifugation with deionized water and ethanol and the product was dried at 60°C under vacuum for 4 h. The obtained sample marked as C--Bi_2MoO_6. In addition, the contrasted samples were synthesized.[1] They were labeled as Bi_2MoO_6-01, Bi_2MoO_6-02, Bi_2MoO_6-03 and Bi_2MoO_6-04, respectively.

Synthetic mechanism:

In the reaction process, the introduction of oleate ions could insure that the ultrathin subunits were generated. Before the solvent heat reaction, the oleate ions and dissociated Bi^{3+} ions in solution rapidly generate the ultrathin Bi-oleate nanosheet complex compound through complexation on which oleate ions are absorbed to reduce the surface energy and promote the formation of an ultrathin structure.[2] Then, the solvent effect from the ethylene glycol/ethanol mixed solution can regulate the self-assembly of the mesoporous hollow structure through a dissolution– recrystallization process (if using water as the solvent, we only fabricate ultrathin Bi_2MoO_6 nanosheets).[3] Due to solvent-induced

Ostwald ripening and oleate ion-induced lamellar intermediate formation, the novel hierarchical nanosheet-assembled Bi_2MoO_6 hollow micronbox and ultrathin subunits were simultaneously realized through this synergistic assembly process. Compared with bulk Bi_2MoO_6 by conventional method, novel hierarchical nanosheet-assembled Bi_2MoO_6 hollow micronbox tructural could prove the importance of these structural features for high-activity photocatalytic property. Particularly, the as-prepared photocatalyst with robust light absorption ability, efficient charge separation and transmission, a broadened optical window and abundant surface active sites are ascribed to the novel hierarchical hollow structure and ultrathin subunits simultaneously. Thereby, the remarkable enhancement of the photocatalytic Nitrogen fixation and dye degradation performance was given in this work.

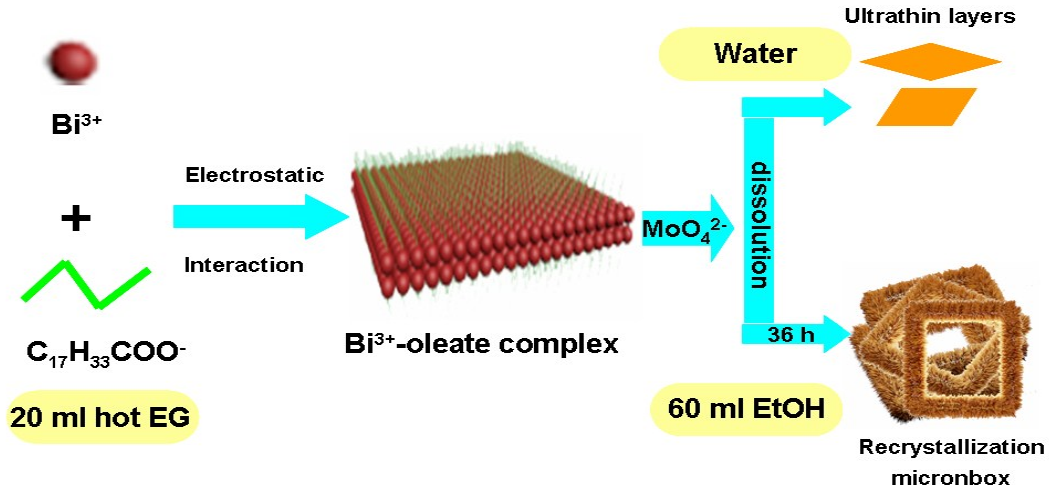

Fig. S1 Schematic illustration of synthetic mechanism with respect to the formation of novel hierarchical nanosheet-assembled Bi2MoO6 hollow micronbox

Photocatalytic activity:

The light source for photocatalytic reaction was a 300 W Xe lamp (PLS-SXE 300, Beijing Perfect Light Co., Ltd). And photocatalytic activities of as-prepared samples were determined by measuring the degradation rate of Rhodamine B dye under visible light irradation and simulated sunlight. We used a cut off filter λ>420 nm to obtain Visible light. Subsequently, 20 mg the sample was dispersed in 50 mL RhB solution (10 mg/L) by sonication for 5 min. Then, solutions were stirred for 30 min in dark for adsorption–desorption equilibrium. In the end, the reaction solution was illuminated using different light sources for degradation of RhB at room temperature naturally. At the given 20 min time intervals, 4 mL suspension was collected and catalyst was separated by centrifuge. Degradation of RhB was monitored by using a UV-visible spectrophotometer. The RhB concentration is marked C after light irradiation for a certain period of time, and C_0 is the fundamental concentration of RhB at adsorption/ desorption equilibrium in dark.[4]

Measurement photocatalytic nitrogen fixation performance.

All the photocatalytic nitrogen reduction experiments were conducted at room temperature; and, under simulated sunlight irradiation. The light source is a 300 W Xe lamp (PLS-SXE 300, Beijing Perfect Light Co., Ltd). For nitrogen reduction, first, 20 mg as-prepared catalysts were added into 100 ml ultrapure water in a reactor, which was

equipped with water circulation. The mixture solution was continuously stirred in the dark with high-purity N_2 bubbled at a flow rate of 50 mL·min-1 for 30 min, subsequent turn on the light and 5 mL of reaction solution was taken out from the reaction in every 30 min and further removing the photocatalyst by using the 0.22 μm filter and the obtained solution was was monitored by Nessler's colorimetry with the UV-vis spectrometer at 420 nm.[5] The monochromatic lightirradiation was obtained by using different band pass filter (380 nm, 420 nm, 450 nm, 475nm, 520nm, 550nm, 600nm and 650nm); and, the total light intensity was measured by optical power meter((Beijing Normal University photoelectric instrument factory, FZ-A). The external quantum efficiency at different wavelength was calculated by using following equation:

$$AQE = \frac{6 \times the\ number\ of\ evolved\ NH_3\ molecules}{the\ number\ of\ incident\ photons} \times 100\%$$

$$= \frac{6 \times Na \times M_{NH_3}}{\frac{PSt\lambda}{hc}}$$

where Na is Avogadro's constant; M_{NH_3} is the mole number of generated NH_3; P is the optical density; S is the light irradiation area; t is the light irradiation time; λ is wavelength of monochromatic light; h is the Planck's constant; and c is the speed of light.

Electrochemical and photocatalytic test

Photoelectrochemical measurements were investigated on a CHI660E electrochemical workstation (Shanghai Chenhua, China) using a three-electrode configuration with the as-prepared samples as working electrodes. The working electrodes were prepared by a dip-coating method: 5 mg of sample was suspended in 0.15 mL ultrapure water. The mixtures were ultrasonically scattered for 20 min to produce a slurry, which was then dip-coated onto a glass carbon electrode and dried under an alcohol environment. Then, 0.5 mol/L sodium sulfate was used as the electrolyte. All investigated electrodes show a similar thickness. The light source was a 300 W Xe lamp (PLS-SXE 300, Beijing Perfect Light Co., Ltd.). The photocurrent response was obtained by potentiostatic (current vs. time, I–t) measurements under intermittent illumination at a bias of 0.7 V vs. Electrochemical impedance spectroscopy (EIS) was conducted using an alternating current signal (10 mV) in the frequency range of 0.1–105 Hz at open circuit potential (OCP). The incident photon to current conversion efficiency (IPCE) was calculated with the following formula.[6]

$$IPCE(\lambda) = 1240j(\lambda)/E(\lambda)\lambda*100$$

where λ, j and E are the wavelength (nm), the photocurrent density, and the incident power of the monochromatic light, respectively. The photocurrent density (j) was determined by measuring current versus

time at a constant potential (1.0 V SCE) and E was investigated with a photometer.

Material characterization

SEM: images were taken using a field-emission scanning electron microscope (JSM-7800F, JEOL).

TEM: The TEM analyses were performed by a JEOL JEM-2100F transmission electron microscope. Light absorption property was evaluated by UV-vis diffuse reectance spectra (UV-vis DRS, CARY 100&300, VARIAN), BaSO4 was used as a reectance standard.

XRD: The crystallinity and the purity of the as-prepared samples were characterized by powder X-ray diffraction (XRD) analysis on a Shimadzu XRD-6100 diffractometer at 40 kV and 40 mA with Cu-Ka radiation.

XPS: Data were recorded at a scan rate of 0.07 s1 in the 2 theta range 10–70°. X-ray photoelectron spectroscopy (XPS) measurements were taken with a Thermo VG ESCALAB-250 system with Al-Ka and Mg-Ka source operated at 15 kV.

UV-vis DRS: Light absorption properties were evaluated using UVvis diffuse reflectance spectra (UV-vis DRS, CARY 100&300, VARIAN), and BaSO4 was used as a rectance standard.

PL: The PL spectra of the photocatalysts were analysed using a Hitachi F-7000 fluorescence spectrophotometer.

BET: The N2-sorption measurements were performed by using a

Micromeritics Tristar 3000 at 77 K, and the pore size distribution was estimated using the Barrett–Joyner–Halenda (BJH) method.

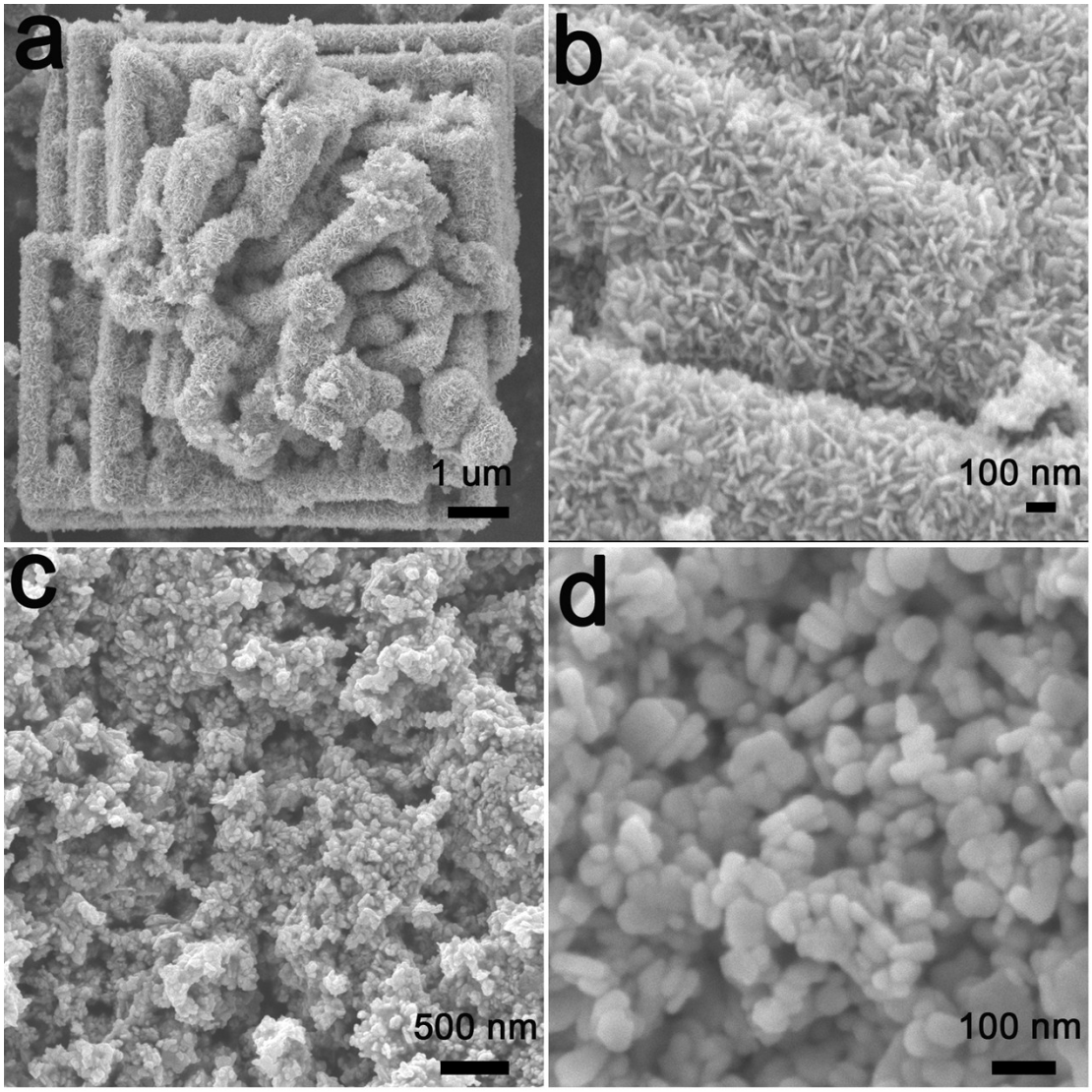

Fig. S2 (a-b) SEM images of B-Bi_2MoO_6; (c-d) SEM images of C-Bi_2MoO_6.

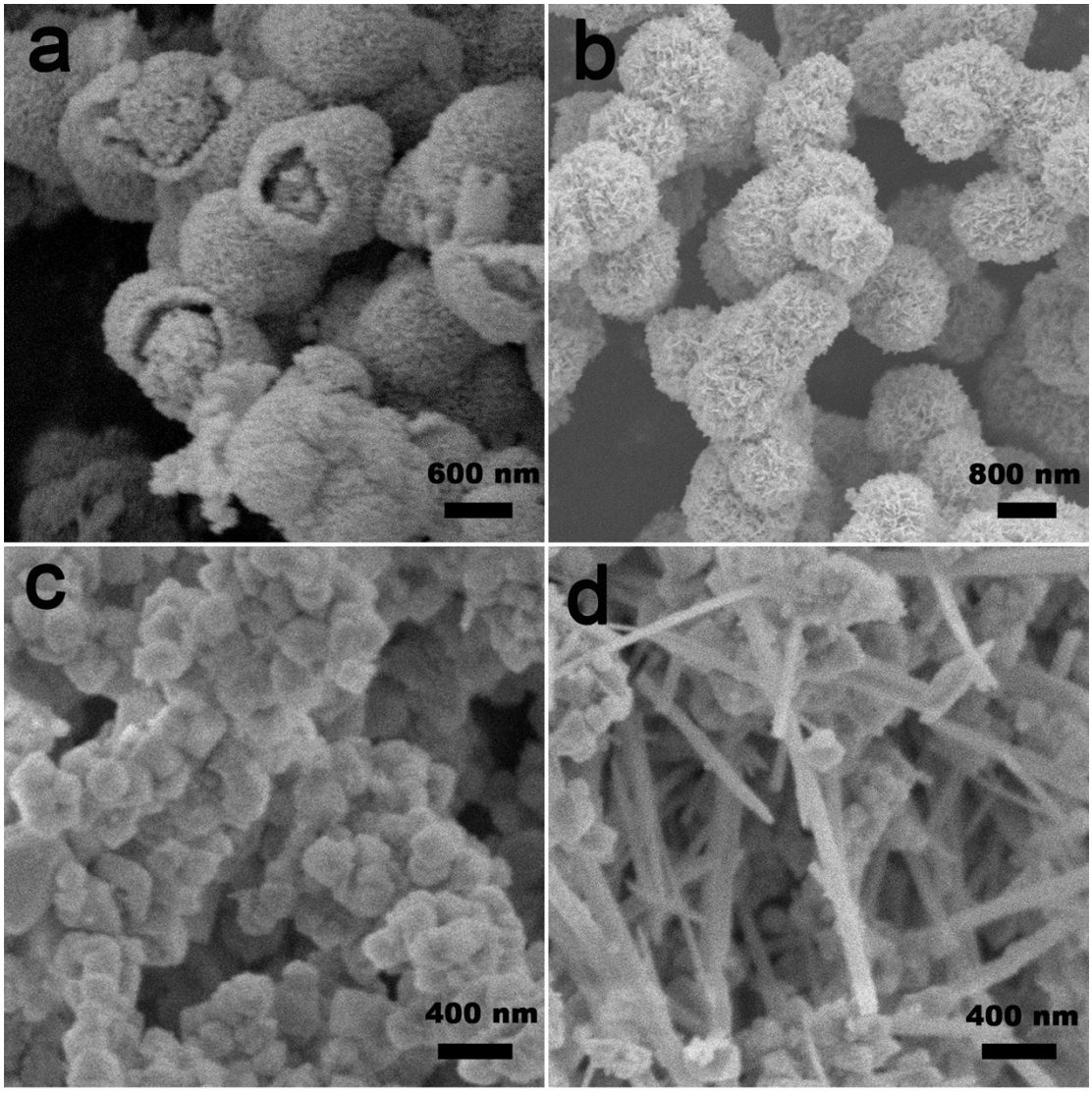

Fig. S3 SEM images of Bi_2MoO_6-01 (a), Bi_2MoO_6-02 (b), Bi_2MoO_6-03 (c), Bi_2MoO_6-04 (d).

It seen that the morphology of both B-Bi_2MoO_6 and C-Bi_2MoO_6 samples is totally different (Fig. S2). The SEM images of the obtained C-Bi_2MoO_6 exhibit that the nano-scale sheets of C-Bi_2MoO_6 are similar size and evenly distributed, but the serious aggregation of nano-sheet. Fig. S3 shows that the morphologies of the Bi_2MoO_6-01, Bi_2MoO_6-02,

Bi_2MoO_6-03 and Bi_2MoO_6-04 are core-shell sphere, Microspheres, bluk and nanorods, respectively.

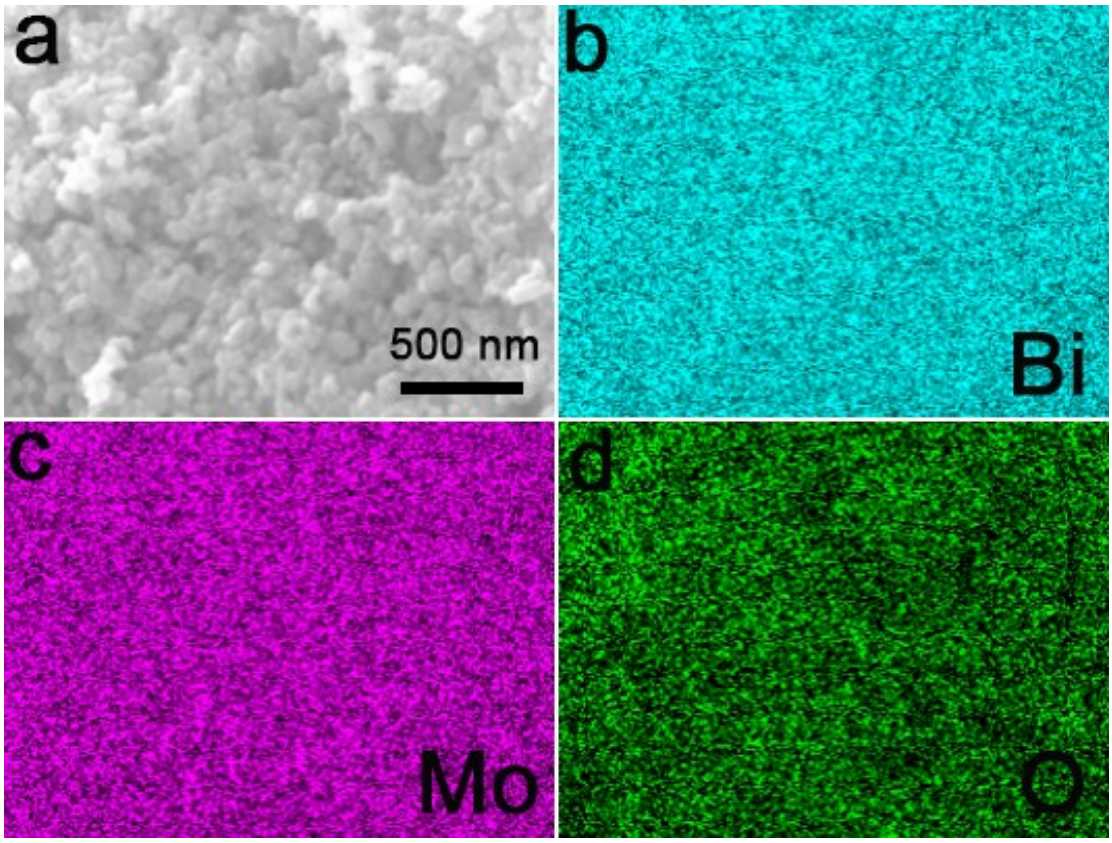

Fig. S4 the EDS mapping image of the as-prepared C-Bi_2MoO_6.

Furthermore, EDS Energy Disperse Spectroscopy was performed to prove prepared pure C-Bi_2MoO_6. It showed as Fig. S4, the as-prepared sample reveals a uniform distribution of Bi, O, Mo elements throughout the material.

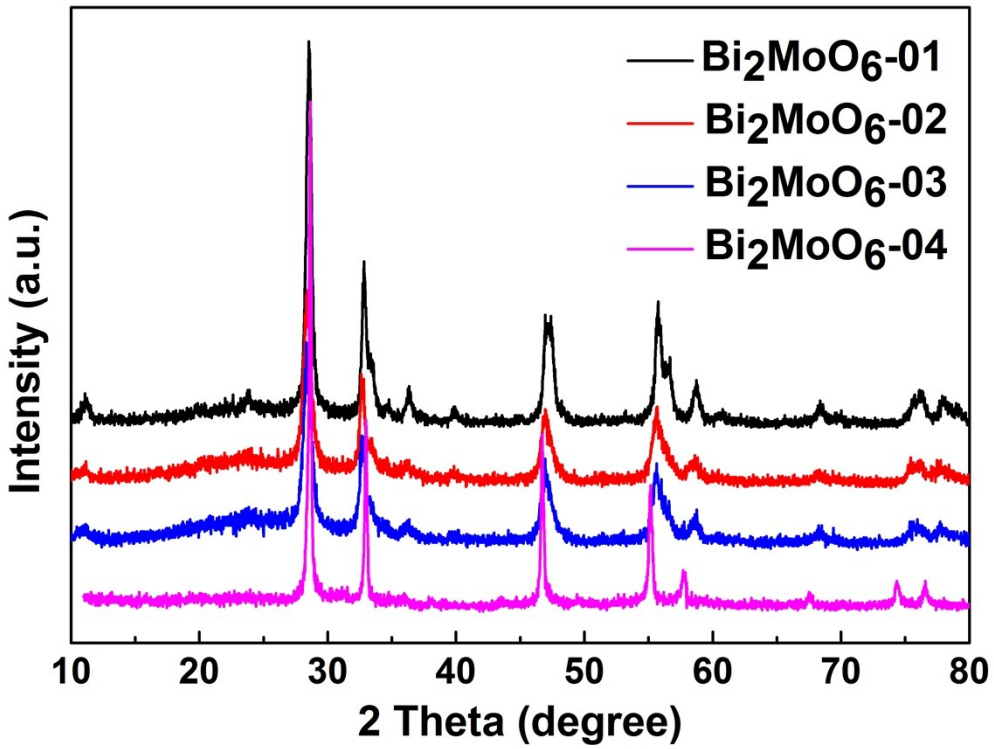

Fig. S5 XRD patterns of the prepared bismuth molybdate samples with different shapes.

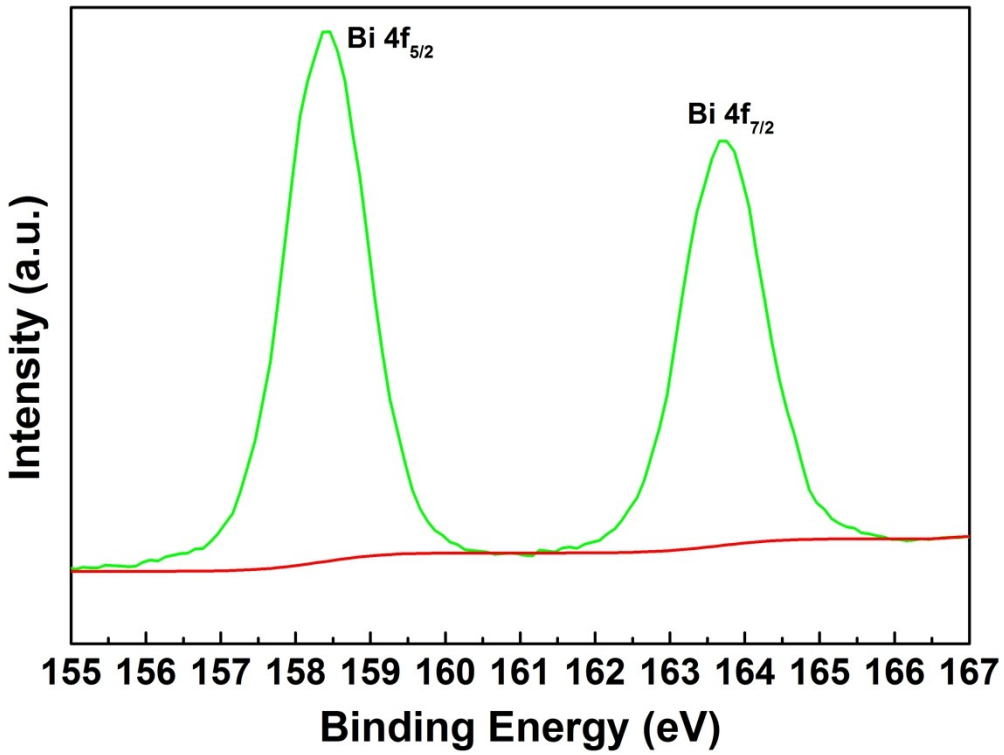

Fig. S6 XPS spectrum of Bi 4f for the sample B-Bi_2MoO_6

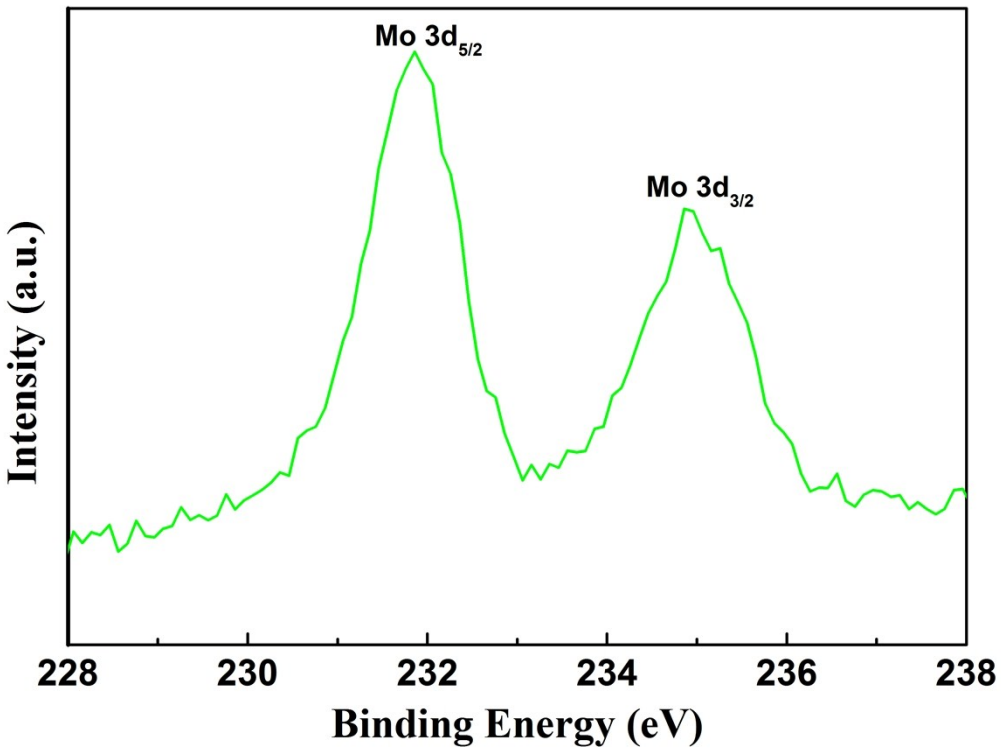

Fig. S7 XPS spectra of Mo 3d for the sample B-Bi_2MoO_6.

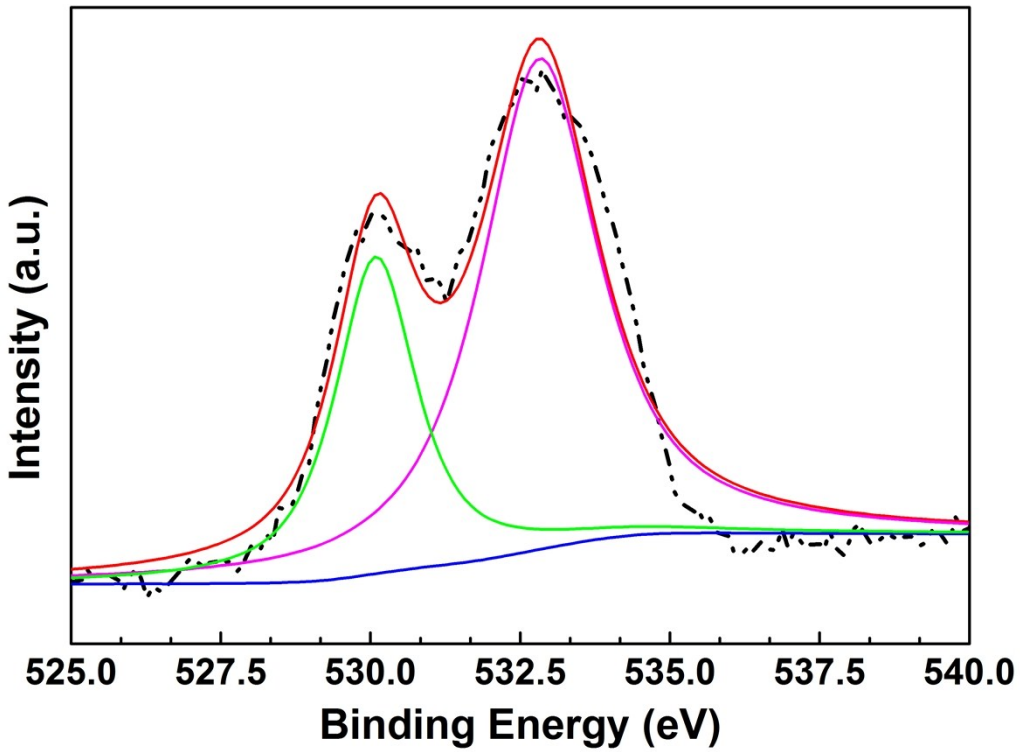

Fig. S8 XPS spectra of O 1s for the sample B-Bi_2MoO_6.

Using X-ray photoelectron spectroscopy (XPS) could describe more detailed information regarding the chemical and bonding environment of the B-Bi_2MoO_6. Fig. S6 shows the high resolution XPS spectra for the Bi 4f region. From Fig. S6, the binding energies at around 231.9 eV and 235.0 eV can be ascribed to Mo 3d. Fig. S8 presents the binding energies of O 1s at around 231.9 eV and 235.0 eV, which is attributed to the lattice oxygen and adsorbed oxygen.[7] All of these results indicated that the heterostructures are prepared of Bi_2MoO_6.

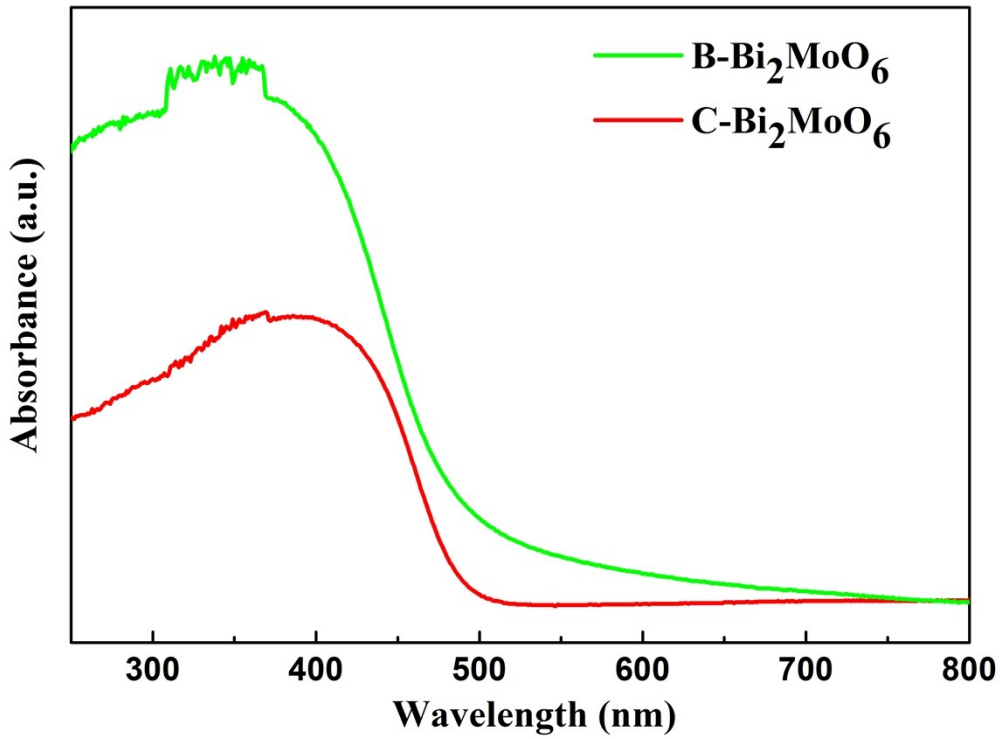

Fig. S9 UV-vis diffuse reflectance spectra of B-Bi_2MoO_6 and C-Bi_2MoO_6.

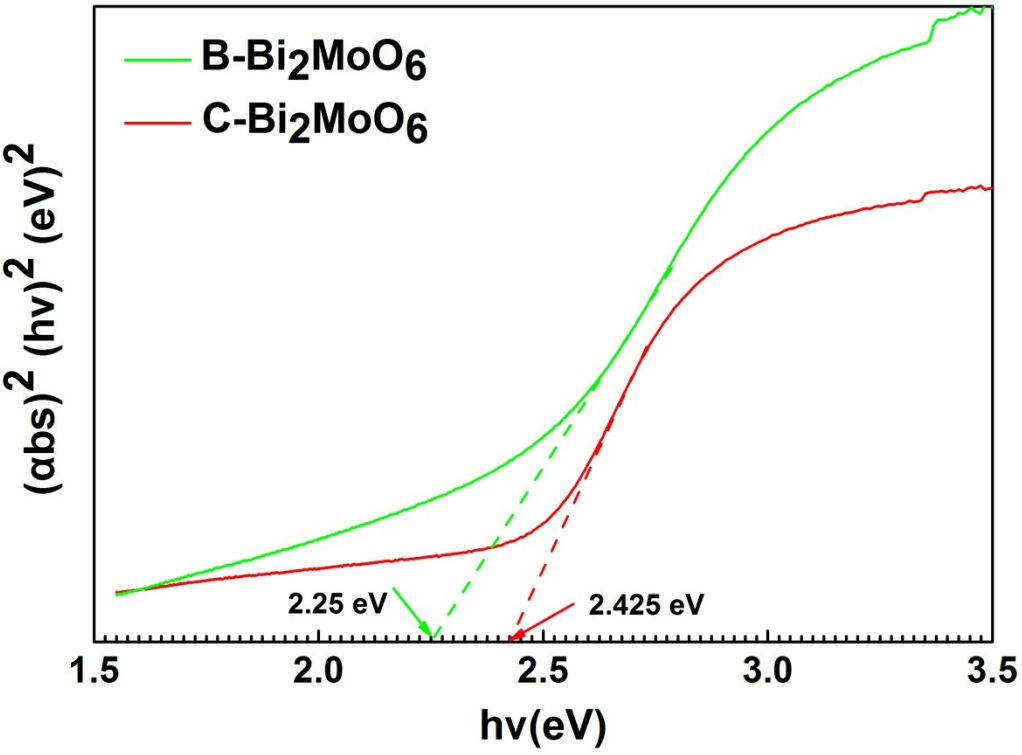

Fig. S10 The corresponding Tauc plots of the as-prepared samples.

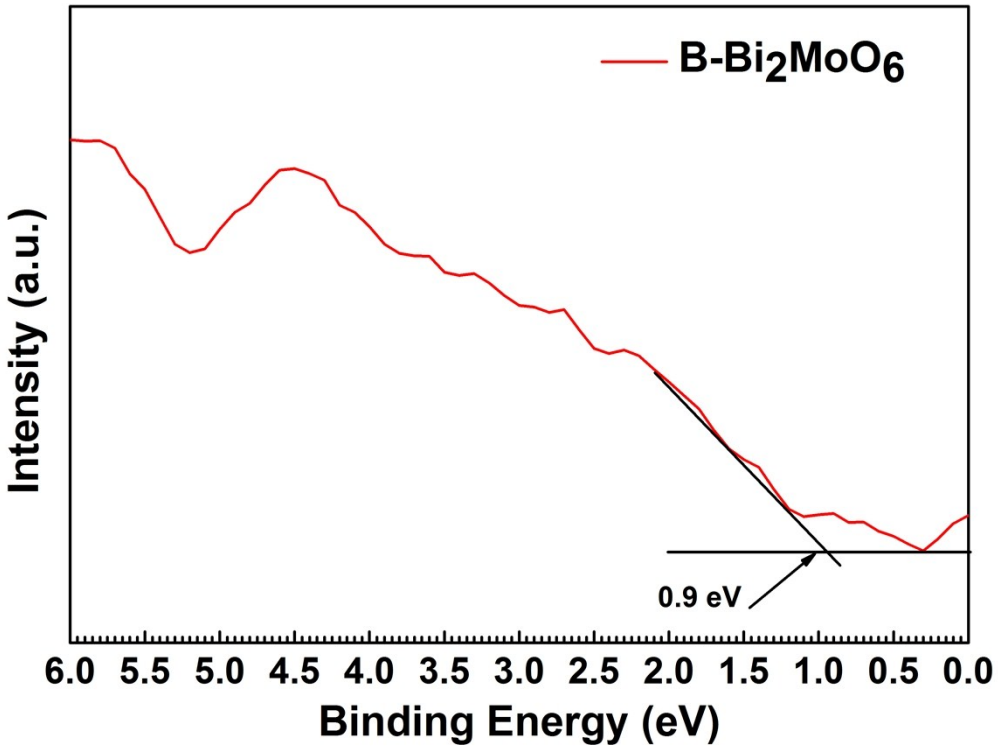

Fig. S11 Valence-band XPS spectra of the Bi_2MoO_6 sample.

Fig. S9 shows UV-vis diffuse reflectance spectra of B-Bi_2MoO_6 and C-Bi_2MoO_6. We can obtain that both photocatalysts exhibit absorption bands in the visible light, revealing the red shift of B-Bi_2MoO_6. Additionally, we can estimate the band gap energy of photocatalyst through the $\alpha hv = A(hv - Eg)^{n/2}$, where, α, v, Eg and A are the absorption coefficient, the light frequency, the band gap and a constant, respectively.[8] Moreover, n decides the characteristics of the transition in a semiconductor. The value of n = 1 or 4 decides the characteristics of the direct and indirect band gap materials, respectively. The optical transitions of Bi_2MoO_6 are direct and the value of n is thus 1. From Fig.

S10, the band gap of B-Bi_2MoO_6 and C-Bi_2MoO_6 was calculated to be about 2.25 eV and 2.425 eV, respectively. As seen in Fig. S11, Valence-band XPS spectra of the Bi_2MoO_6 sample reveals that valence band of the as-prepared B-Bi_2MoO_6 was calculated to be approximate 0.9 eV. Valence-band (VB)-XPS combined with the corresponding Tauc plots analysis is a method to determine the conduction band (CB) and VB positions. The CB positions of B-Bi_2MoO_6 was calculated based on the band gaps to be –1.35 versus the normal hydrogen electrode.[9] Fortunately, it can be seen that the CB positions of B-Bi_2MoO_6 sample are higher than E0 (N_2/NH_3 = -0.28 V vs NHE).[10] Thus, it indicates that B-Bi2MoO6 can reduce N_2 to NH_3 based on thermodynamics.

$$N_2 + 2H_2O + 6H+ + 6e– = 2NH_3•H_2O$$

($E_0(N_2/NH_3)$ = –0.276 V vs NHE) [10]

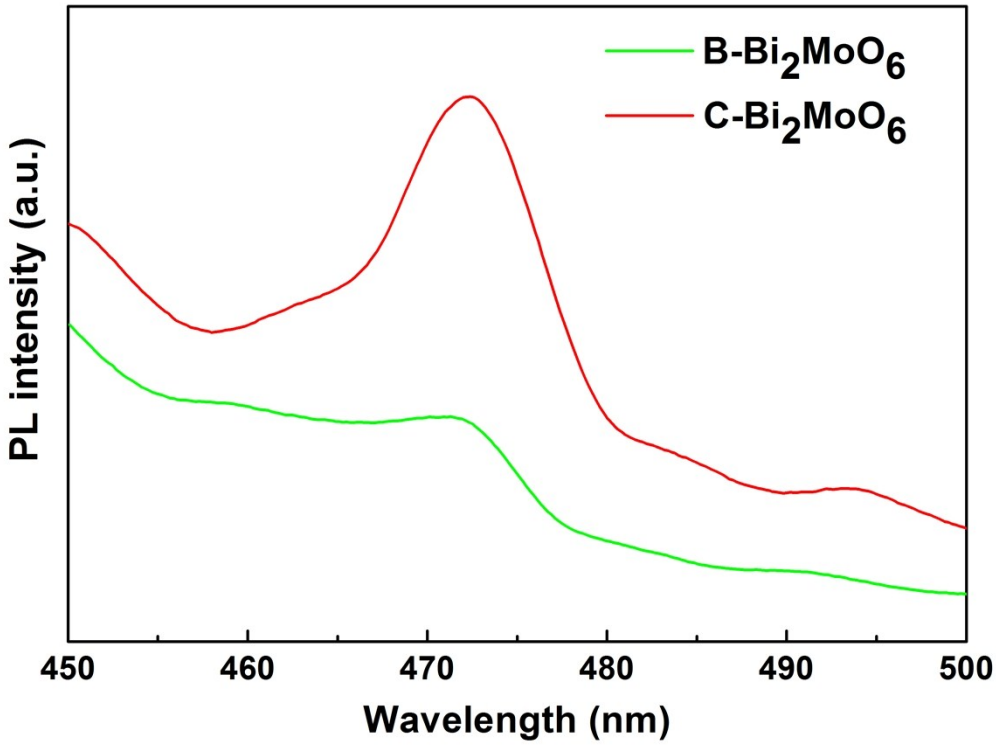

Fig. S12 The PL spectra of as-prepared samples.

To investigate the separation and dynamic processes of the photo-generated carriers, PL spectroscopy was conducted with 430 nm excition. The PL spectra B-Bi_2MoO_6 and C-Bi_2MoO_6 exhibit a strong emission peak at around 472 nm, which is mainly assigned to the emission of the band-gap transition (Fig. S12).[11] In particular, the emission peak intensity significantly reduced, which means the effective enhancement of the charge separation efficiency. It indicates that the B-Bi_2MoO_6 process the

lower electrons-holes recombination than the conventional C-Bi_2MoO_6 semiconductor.

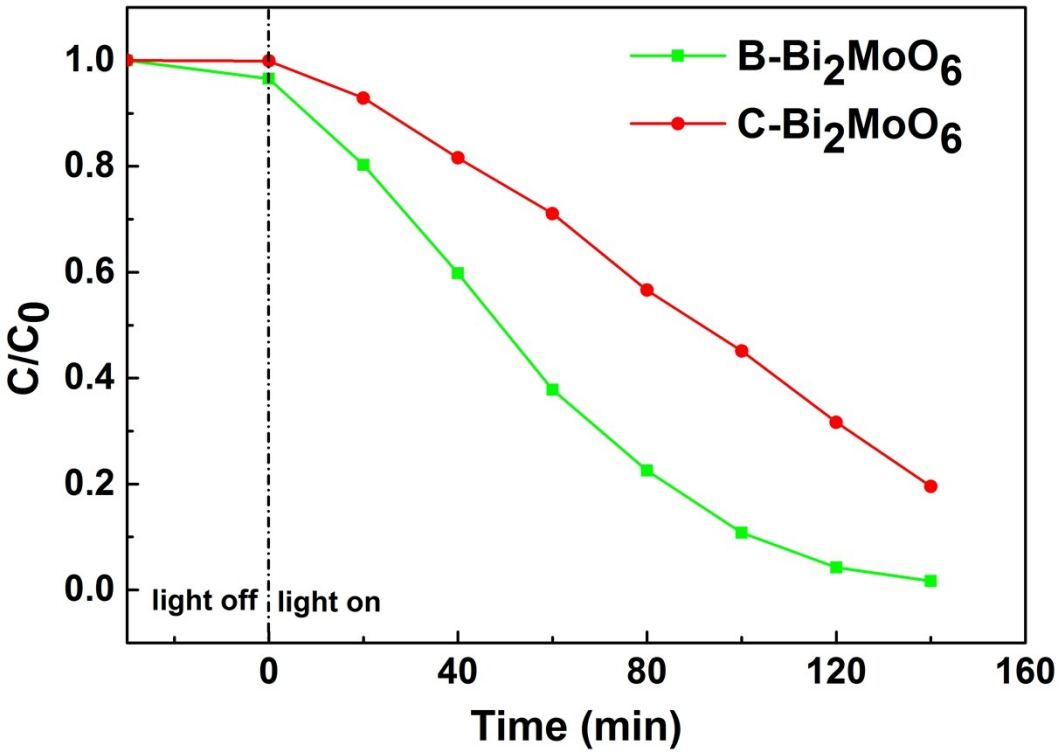

Fig. S13 the degradation curves of RhB under visible light irradiation (a cut off filter > 420 nm)

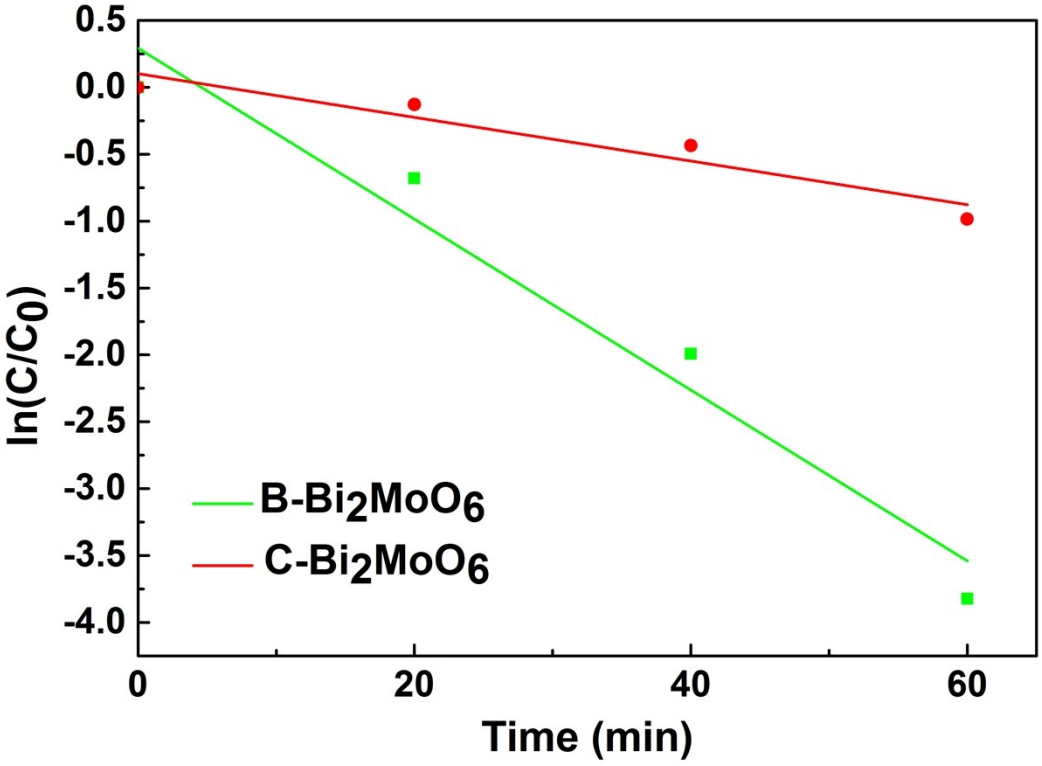

Fig. S14 the $\ln(C/C_0)$ curves of RhB under simulated sunlight irradiation.

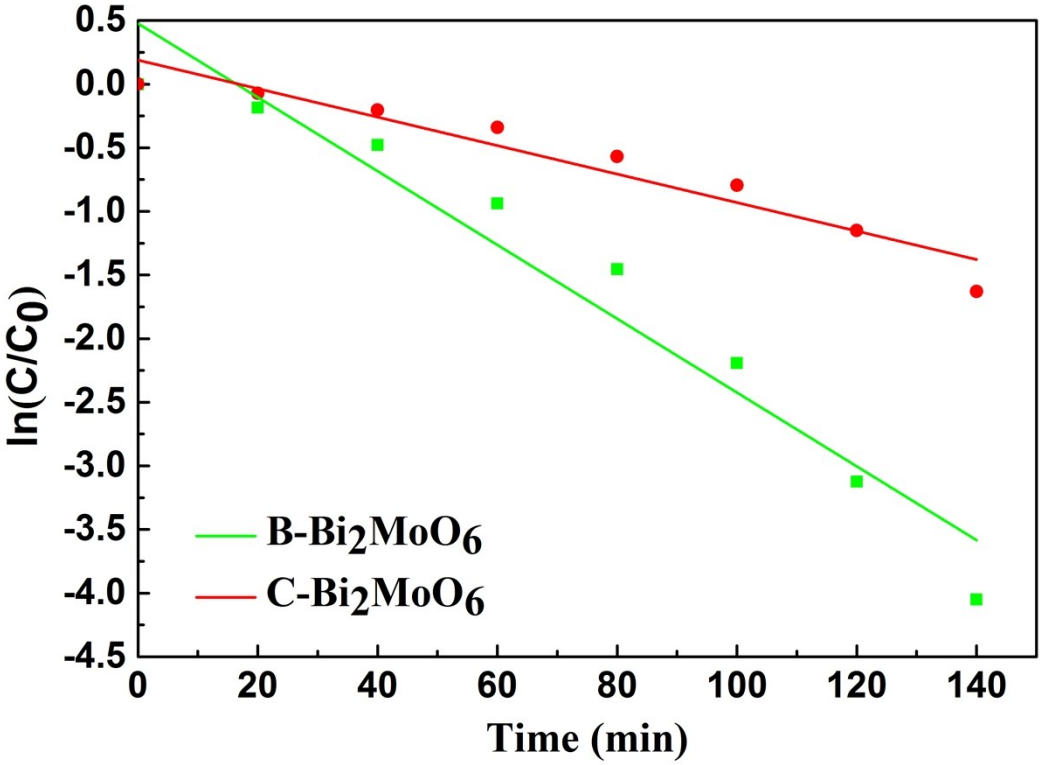

Fig. S15 the $\ln(C/C_0)$ curves of RhB under visible light irradiation (a cut off filter > 420 nm)

Photocatalytic degradation performance of B-Bi_2MoO_6 and C-Bi_2MoO_6 were evaluated by the degradation of RhB in the aqueous solution under visible light illumination (Fig. S13). When adopting B-Bi2MoO6 and C-Bi_2MoO_6 as the photocatalyst, 99% and 80% of RhB were degraded within 140 min. The obtained B-Bi_2MoO_6 displayed higher photocatalytic activity than the C-Bi_2MoO_6. As shown in Fig. S14-S15, the rate constant k was estimated from ln(C/C0) = kt, where k is the rate constant (min^{-1}).[5] Moreover, the rate constant k of the B-Bi_2MoO_6 under visible light and simulated sunlight irradiation is 0.02914 min^{-1} and

0.0637 min^{-1}, respectively, which is about 2.2 and 3.8 times higher than that of C-Bi_2MoO_6.

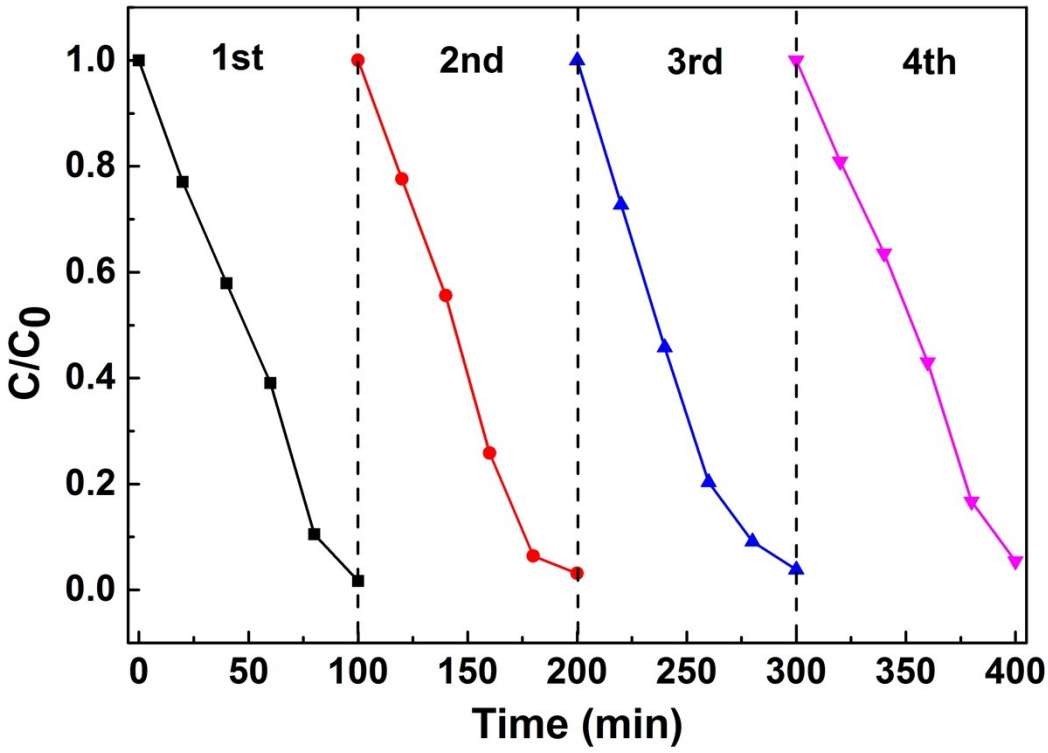

Fig. S16 Cycling runs for the photocatalytic degradation of RhB over B-Bi_2MoO_6 under simulated solar irradiation

To investigate the stability of as-prepared B-Bi_2MoO_6 photocatalyst, we performed the cycling experiments for photodegrading RhB over the B-Bi_2MoO_6 photocatalyst under simulated solar illumination (Fig. S16). The degradation rate of RhB still remained stable after reusing it for four cycles, indicating that B-Bi_2MoO_6 exhibited quite a good stability in the photocatalytic reaction process.

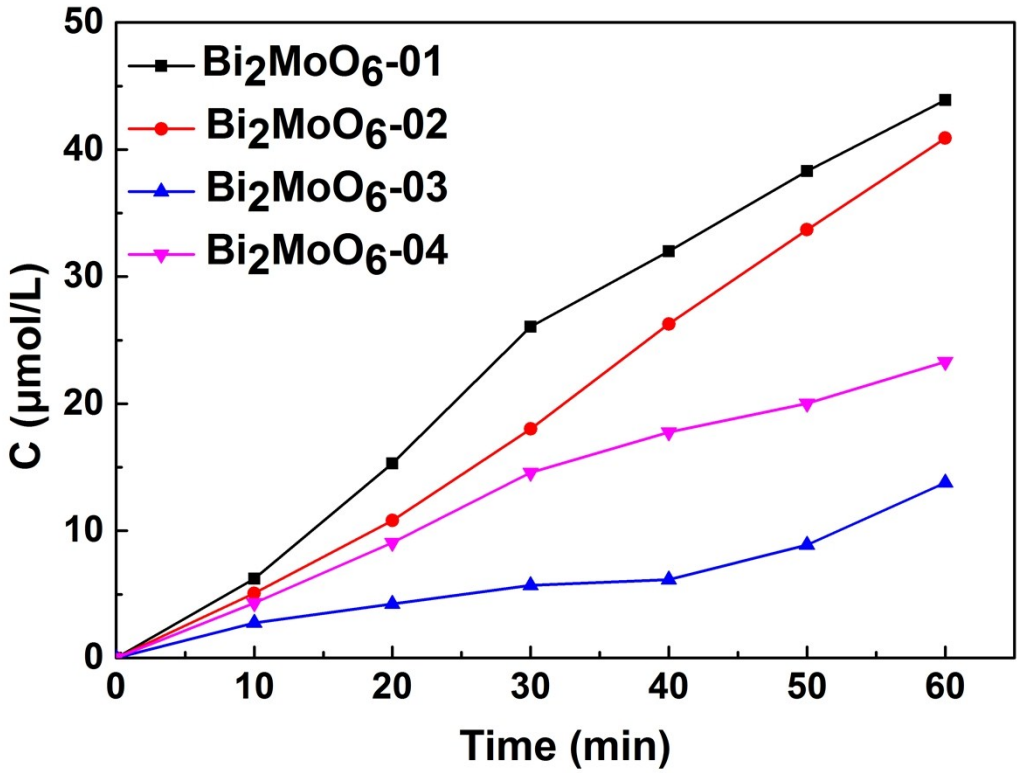

Fig. S17 N_2 fixation of the contrasted samples.

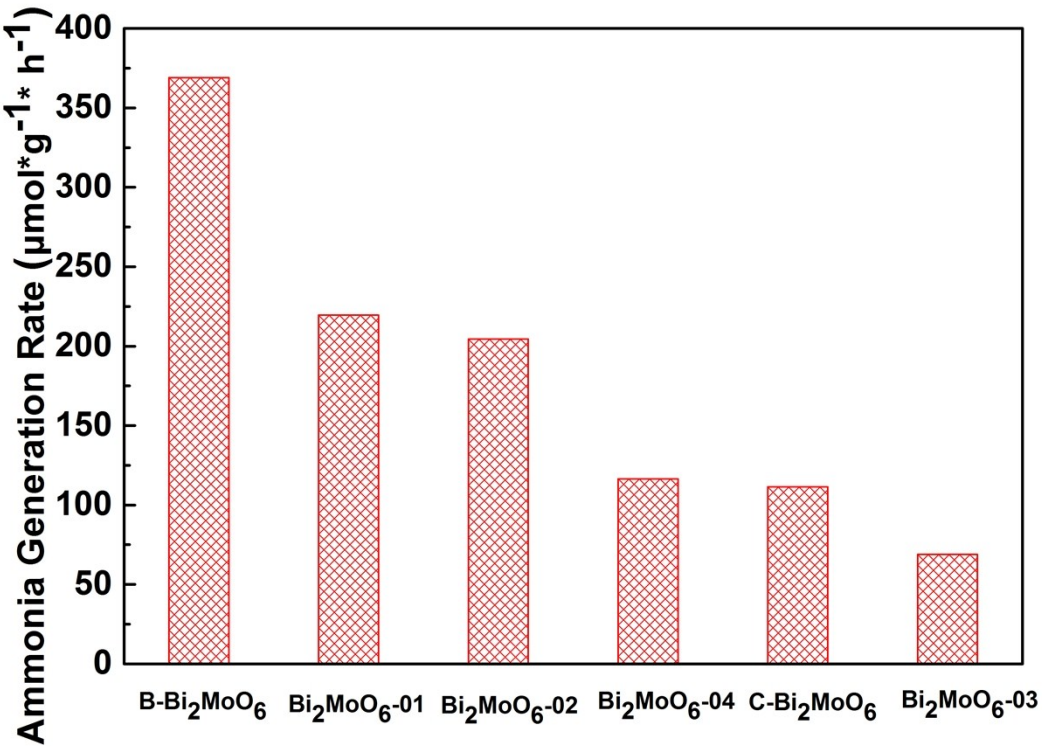

Fig. S18 the ammonia generation rate of the as-prepared samples under simulated solar light.

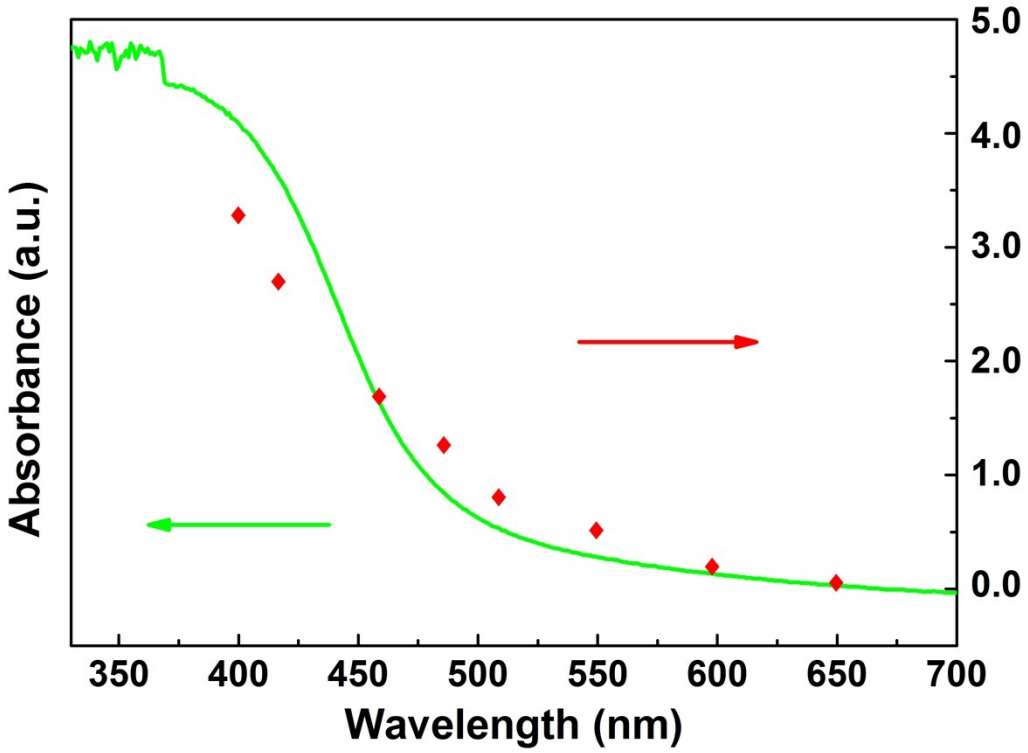

Fig. S19 wavelength-dependent apparent quantum efficiency of light-driven nitrogen fixation from N_2 by H-Bi_2MoO_6 under monochromatic light irradiation.

Table S1 Photocatalytic N_2 fixation over different photocatalysts under various reaction conditions.

Catalyst	Reaction medium	Scavenger	Light Source	NH_3 generation rate (g^{-1})	Reference
B-Bi_2MoO_6	H_2O(1),20℃, High pure N_2	No	300w Xenon lamp, Fell Spectrum	365.0 μmol/h	This work
C-Bi_2MoO_6	H_2O(1),20℃, High pure N_2	No	300w Xenon lamp, Fell Spectrum	111.4 μmol/h	This work
Pt-$SrTiO_3$	H_2O(1),38℃, High pure N_2	No	100w high/pressure mercury lamp, Fell Spectrum	8.0 μmol/h	S12
Fe/doped TiO_2	H_2O(1),25℃, High pure N_2	No	360w Hg/Arc lamp, Fell Spectrum	11.5 μmol/h	S13
Pt/ TiO_2	H_2O(1),25℃, High pure N_2	No	100w high/pressure mercury lamp, Fell Spectrum	9.3 μmol/h	S12
Iron titanate	H_2O(1), High pure N_2	Ethanol	high/pressure Hg lamp, λ>320 nm	11.3 μmol/h	S14
{010} facets of BiOCl	H_2O(1),25℃, High pure N_2	25% Methanol	500w Xenon lamp, Fell Spectrum	92.4 μmol/h	S15
Ru/TiO_2	H_2O(1), alkaline High pure N_2	Ascrorbic acid	250w Xenon lamp, Fell Spectrum	13.6 μmol/h	S16
Pt/ CdS	H_2O(1), 38℃High pure N_2	No	100w high/pressure mercury lamp Fell Spectrum	16.3μmol/h	S12
Fe_2O_3	H_2O(1),29-30℃	No	150w Xenon lamp, Fell Spectrum	10.0 μmol/h	S17
RuO_2/NiO/$BaTiO_3$	H_2O(1),50℃High pure N_2	No	400w high/pressure mercury lamp Fell Spectrum	2.6 μmol/h	S18

Ru/ TiO_2	H_2O(1), alkaline High pure N_2	No	150w Xenon lamp, Fell Spectrum	29.4 μmol/h	S16
$Fe_2O_3(H_2O)_n$	H_2O(1),26℃ PH=10	No	100w tungsten filament, Fell Spectrum	10,0 μmol/h	S19

References

1 J. L. Li, X. J. Liu, X. Q. Piao, Z. Sun and L. K. Pan, RSC Adv., 2015, **5**, 16592; Y. S. Xu and W. D. Zhang, Dalton Trans., 2013, **42**, 1094; D. M. Chen, Q. Hao, Z. H. Wang, H. Ding and Y. F. Zhu, CrystEngComm, 2016, **18**, 1976

2 L. Liang, F. C. Lei, S. Gao, Y. F. Sun, X. C. Jiao, J. Wu, S. Qamar and Y. Xie, Angew. Chem., Int. Ed., 2015, **54**, 13971; Y.C. Hao, X.L. Dong, X. Y. Wang, S. R. Zhai, H.C. Ma and X. F. Zhang, RSC Adv., 2016, **6**, 35709

3 G. H. Tian, Y. J. Chen, W. Zhou, K. Pan, Y. Z. Dong, C. G. Tian and H. G. Fu, J. Mater. Chem., 2011, **21**, 887

4 H. B. Liu, H. L. Hou, F. M. Gao, X. H. Yao and W. Y. Yang, ACS Appl. Mater, 2016, **8**, 1929.

5 Y. Bai, L. Q. Ye, T. Chen, L. Wang, X. Shi, X. Zhang, and D. Chen, *ACS Appl. Mater. Interfaces*, 2016, **8** (41)

6 L. W. Zhang, C. Y. Lin, V. K. Valev, E. Reisner, U. Steiner and J. J. Baumberg, Small, 2014, **19**, 3970.

7 G. X. Zhang, S. H. Sun, D. Q. Yang, J. P. Dodelet and S. Edward, Carbon, 2008, 46, 196.

8 G. H. Tian, Y. J. Chen, W. Zhou and K. Pan, J. Mater. Chem., 2011, **21**, 887–892; J. Zhang, F. J. Shi, D. F. Chen, J. M. Gao, Z. X. Huang, X. X. Ding and C. C. Tang, Chem. Mater., 2008, **20**, 2937.

9 K. Chang, X. Hai, H. Pang, H. B. Zhang, L. Shi, G. G. Liu, H. M. Liu, G. X.

Zhao, M. Li, J. H. Ye, Adv. Mater. 2016, **28**, 10033.; Y. Bai, L. Q. Ye, T. Chen, L. Wang, X. Shi, X. Zhang, D. Chen, ACS Appl. Mater. Interfaces, 2016, **8**, 27661.

10 H. Wang, Y. Su, H. X. Zhao, H. T. Yu, S. Chen†, Y. B. Zhang, and X. Quan, Environ. Sci. Technol. 2014, **48**, 11984-11990

11 H. C. Ma, L. X. Yue, C. L. Yu, X. L. Dong, X. X. Zhang, M. Xue, X. F. Zhang and Y. H. Fu, J. Mater. Chem, 2012, **22**, 23780.

12 H. Miyama,N.Fujii, Y.Nagae, Chem. Phys. Lett.,1980, **74**, 523.

13 G. N.Schrauzer, T. D.Guth, J. Am. Chem. Soc.,1977, **99**, 7189.

14 O.Rusina, A.Eremenko, G.Frank, H. P.Strunk, H.Kisch,Angew. Chem. Int. Ed. Engl., 2001, **40**, 3993.

15 H. Li, J. Shang, J. S. Shi, K. Zhao, L. Z. Zhang, Nanoscale, 2016, **8**, 1986.

16 K. T.Ranjit, T. K.Varadarajan, B.Viswanathan, J. Photochem. Photobiol. A Chem.,1996, **96**, 181.

17 M. M. Khader, N. N. Lichtin, G. H. Vurens, M. Salmeron,; G. A. Somorjai, Langmuir 1987, **3**, 303.

18 Q. Li, K. Domen, S. Naito, T. Onishi, K. Tamaru, Chem. Lett.,1983, **2**, 321.

19 K. Tennakone, S. Wickramanayake, C. A. N. Fernando, O. A. Ileperuma, S. J. Punchihewa, Chem. Soc. Chem. Commun. 1987, **14**, 1078.